Synthesis, characterization, and computational survey of a novel material template o-xylylenediamine

Meriam Tahenti, Noureddine Issaoui, Thierry Roisnel, Houda Marouani

▶ **To cite this version:**

Meriam Tahenti, Noureddine Issaoui, Thierry Roisnel, Houda Marouani. Synthesis, characterization, and computational survey of a novel material template o-xylylenediamine. Journal of the Iranian Chemical Society, 2022, 19 (4), pp.1499-1514. ⟨10.1007/s13738-021-02392-9⟩. ⟨hal-03367773⟩

HAL Id: hal-03367773

https://hal.science/hal-03367773v1

Submitted on 26 Oct 2021

HAL is a multi-disciplinary open access archive for the deposit and dissemination of scientific research documents, whether they are published or not. The documents may come from teaching and research institutions in France or abroad, or from public or private research centers.

L'archive ouverte pluridisciplinaire **HAL**, est destinée au dépôt et à la diffusion de documents scientifiques de niveau recherche, publiés ou non, émanant des établissements d'enseignement et de recherche français ou étrangers, des laboratoires publics ou privés.

Distributed under a Creative Commons CC BY-NC 4.0 - Attribution - Non-commercial use - International License

Synthesis, characterization, and theoretical studies of a new hybrid material template *o*-xylylenediamine

Meriam Tahenti[a], Noureddine Issaoui[b], Thierry Roisnel[c], Houda Marouani[a]

[a]Université de Carthage, Faculté des Sciences de Bizerte, LR13ES08 Laboratoire de Chimie des Matériaux, 7021, Bizerte,Tunisie
[b]University of Monastir, Laboratory of Quantum and Statistical Physics LR18ES18, Faculty of Sciences, Monastir 5079, Tunisia
[c]Univ Rennes, CNRS, ISCR (Institut des Sciences Chimiques de Rennes) – UMR 6226, F-35000 Rennes, France

*Correspondence e-mail: houdamarouani2015@gmail.com

Abstract

A new salt Bis(*o*-xylylenediammonium) tetrachloride monohydrate, $(C_8H_{14}N_2)_2Cl_4.H_2O$, produces a novel centrosymmetric organic–inorganic compound synthesized in an aqueous solution by slow evaporation technique. This compound has been crystallized in the orthorhombic space group *P*nma and the following parameters obtained are a=9.0677(9) Å, b=24.282 (2) Å, c=9.4726 (8) Å, V=2085.7 (3)Å^3 and Z=4, at 150 K, it is characterized by X-ray diffraction, infrared, fluorescence and UV-Vis spectroscopy. The crystal packing is governed by the N–H···Cl, O–H···Cl hydrogen bonding interactions between the organic network and the inorganic one, which stabilize the crystal packing. Moreover to gain an insight into the behavior of these interactions, Hirshfeld surfaces analysis have been investigated. Theoretical calculations were performed using density functional theory (DFT) and were made by comparison with the experimentally determined structure to study the molecular structure with geometrical optimization, electronic and topological properties of OXDACl at B3LYP/6-311++G(d,p) level.

Keywords: Single crystal X-ray diffraction, photoluminescence, Hirshfeld Surface, RDG, DFT.

1. Introduction

Ionic organic-inorganic salts have received a lot of attention in recent years due to their noncovalent interactions, such as hydrogen bonding, that play significant roles in various fields ranging from molecular recognition [**1**], host–guest chemistry [**2**], crystal engineering

ACCEPTED MANUSCRIPT - CLEAN COPY

[**3**], supramolecular chemistry [**4**], biochemistry [**5**] and pharmaceutical chemistry [**6**] to materials science.

Xylylenediamine and its derivatives have been of great interest due to their possessing of valuable pharmacological properties [**7**], which have been evaluated by antimicrobial studies against various bacteria and fungi species, cytotoxicity against cancer cells and good antioxidant activity [**8**].

Here, o-xylylenediamine organic molecules where the two ammonium groups are in ortho position which can be associated with chloride anions to produce systems with a potentially forceful network of hydrogen bond interactions.

The role of weak intermolecular interactions in the determination of crystal structures is one of the principal avenues of investigation now being probed in crystal engineering studies. Interactions such as hydrogen bonding and π–π stacking play a very important role in the organization of structural units in areas ranging from biochemistry to material science.

For several years numerous research works have been devoted to the preparation of hybrid salt materials. In this article, we report a crystal o-xylylenediammonium chloride, its Hirshfeld surface analysis and a physicochemical characterization. The crystal packing is an organic salt network constructed by hydrogen bonds. The contact enrichments were computed by Hirshfeld surface analysis in order to evaluate which contacts play major roles in the stabilization of the crystal packing.Intermolecular interactions were studied by AIM and RDG analyses, infrared spectroscopy, Fluorescence and UV-vis spectroscopy of a novel hybrid organic-inorganic compound have been investigated.

2. Experimental

2.1. Synthesis and crystallization

Products and solvents were obtained from Sigma Aldrich Company. The chemical synthesis of the title compound $(C_8H_{14}N_2)_2Cl_4{\cdot}H_2O$ was carried by adding of HCl (37%) to the ethanol solution of ortho-xylylenediamine. The solution was stirred for 1h and left to stand in the open air. After 1 week of slow evaporation, colorless prismatic form crystals stable at room temperature formed at the bottom of the crystallizer. The typical size of the crystals is 0.50 × 0.31 × 0.19 mm.

2.2. Materials and Physical measurements

X-ray diffraction measurements were made at 150 K using a diffractometer Bruker-AXS APEXII, employing monochromated MoKα radiation (λ = 0.71073 Å). Absorption corrections were

ACCEPTED MANUSCRIPT - CLEAN COPY

performed using multi-scan technique using SADABS program [**9**]. Amongst 10803 measured reflections only 2430 are independent and 2269 with intensity $I > 2\sigma(I)$ on the range (2.3°-27.5°). The crystal structure was solved by the direct method and refined via full-matrix least-squares techniques using the SHELXL package [**10**] across the assist of the WINGX program [**11**] with all non-hydrogen atoms anisotropic. All the hydrogen carbon atoms were situated in geometrically optimized positions and treated as riding atom, apart from those bound to N and O atoms which were found in the difference map and refined isotropically**.** The drawing of the molecular structure was made with DIAMOND program [**12**]. A final refinement on F^2 converged at $R(F^2) = 0.032$ and $wR(F^2) = 0.082$. Further details of the structure analysis are given in Table **1**. An ORTEP drawing of the molecular arrangement is exposed in **Fig. 1a**.

IR spectrum was recorded in the range 4000−400 cm^{-1} with a Perkin-Elmer FT-IR 1000 spectrometer dispersed with KBr using the technique of pellets. Solid state UV-Vis absorption spectra were obtained by a PerkinElmer Lambda 35 spectrophotometer in the range of 200-800 nm. Emission spectrum was obtained on a PerkinElmer LS55 fluorescence spectrometer equipped with a 450 W xenon lamp as the excitation source using solid sample at room temperature.

2.3. Computational details

All DFT calculations were performed starting from the experimental single-crystal X-ray software (cif file) and was optimized with the DFT method accomplished in the gas using the Gaussian 09 program [**13**]. The calculations were performed using the hybrid B3LYP functional [**14**] and the standard 6-311+G(d,p) basis set. The vibrational assignments were performed considering the potential energy distribution components (PED) ≥ 10% using the VEDA4 package [**15**]. The GaussView molecular visualization program [**16**] was used to verify the assignments of the bands.

Three-dimensional (3D) Hirshfeld surfaces (HS) and associating two-dimensional (2D) fingerprint maps were used for the visualization and understanding of intermolecular interactions and were drawn using the CrystalExplorer 3.1 program [**17**] imported on a CIF file. Vibrational frequency calculations were then performed at the same level of theory of the optimized geometries to confirm that there are no imaginary frequencies. Multiwfn program [**18**], in accordance with Bader's theory [**19**], was used to determine the topological analysis of noncovalent interaction while the reduced density gradient of the compound are mapped by Multiwfn and plotted by the VMD program [**20**].

ACCEPTED MANUSCRIPT - CLEAN COPY

3. Result and discussion

3.1. X-ray diffraction

The title compound crystallizes in the centrosymmetric orthorhombic space group Pnma with the following unit cell dimensions: a = 9.0677(9) Å, b = 24.282(2) Å, c = 9.4726(8) Å, and Z = 4 (**Table 1**). The asymmetric unit of the title material $(C_8H_{14}N_2)_2Cl_4{\cdot}H_2O$ depicted in an ORTEP drawing, contains one diprotonated o-xylylenediammonium, three chloride anions and one water molecule (**Fig. 1a**). It is worth noting that atoms Cl2, OW1, H1W1 and H2W1 were situated in special positions.

The packing of $(C_8H_{14}N_2)_2Cl_4{\cdot}H_2O$, viewed along the a-axis (**Fig. 2a**), shows that the compound is built up by a succession of cationic and anionic layers, which alternate along the b-axis, the junction of these layers is ensured by hydrogen bonds types N-H…Cl.

In this structure, the chloride anions are associated together in pairs through two O–H…Cl hydrogen bonds, generated by water molecule and form $[(Cl)_2{\cdot}H_2O]^{2-}$ clusters (**Fig. 2b**). These clusters are interconnected *via* N–H…Cl hydrogen bonds to build an infinite layer parallel to the ac plane at *z* = ¼ and 3/4.

Fig. 2c shows that the distribution of organic cations is in a zigzag in z=1/4 and 3/4 planes. The distances between adjacent o-xylylendiammonium cations are 3.40 Å and 3.843 Å, indicating the presence of π…π interactions (**Fig. 3)**, then forming an infinity of inclined chains along the a axis. Assessment of the organic geometrical features (**Table 2**) shows that the o-xylylenediammonium cation exhibits a normal spatial configuration with C-C average distances of 1.420(2) Å and around 1.497(2) Å for C-N distances. The angles C-C-C and N-C-C spread respectively within the ranges 118.6(1) °-123.1(1) ° and 110.8(1) ° and 112.2(1) °, quite similar to those found in other xylylenediamine derivatives para and meta **[21-24**].

Both ammonium goups cation adopt a *trans* conformation with respect to the benzene ring. The same conformation was observed in other related crystal structure $(C_8H_{14}N_2)_2(CdCl_6)$ [**23**]. The *cis* conformation has been observed in $(C_8H_{14}N_2)(NO_3)_2$ [**24**].

Within the structure all the chloride anions are involved as acceptors to form an infinite three-dimensional network, their distances $d_{N\cdots Cl}$ are varying between 3.177 (1)Å and 3.241 (1)Å and $d_{O\cdots Cl}$ between 3.197 (2) Å and 3.325 (2) Å (**Table 3**).

Inside this arrangement (**Fig. 4**), the entities are interconnected via multiple hydrogen bonds generate rings forming $R_4^2(8)$ motif providing stability of the synthesized compound.

DFT calculations were applied on OXDACl at B3LYP/ 6-311++G(d,p) level in order to estimate the effect of intermolecular interactions on geometrical parameters**.** The optimized structure of the compound was performed using Gaussian program [**13**] and their interface

ACCEPTED MANUSCRIPT - CLEAN COPY

Gauss view [**16**] is shown in **Fig. 1b**. The structural parameters obtained by the DFT method for the studied compound are given in **Table 2** compared with experimental results. It is noticing that there is not a big difference between the experimental and theoretical bond lengths, the C-C bond lengths vary from 1.3913-1.5155. The linkage lengths of the methyl groups bound to N are, N1-C2 = 1.5208 Å and N10-C9= 1.4934 Å, which are close to the observed XRD values of about 1.497 Å. These interactions are studied, afterward, using the Hirshfeld surface analysis. The C-C-C binding angles forming the o-xylylenediammonium ring were calculated between 117.34°-123.47° and 114.32°-113.87 for N-C-C. By comparison between the theoretical and experimental binding angles there is a slight difference. This difference is due to that the theoretical calculations were performed in the gas phase where the molecules are isolated while experimental results belong to molecules in solid-state, where the crystal structure is related to intermolecular interactions, despite that the optimized parameters represent a good approximation.

3.2. Hirshfeld Survey

The Hirshfeld surface of the molecule is used in order to visualize and explain the intermolecular interactions present in the crystal. Hirshfeld surface analysis [**25**] and their associated 2D fingerprint plots [**26**] were performed using the software CrystalExplorer 3.1 program [**17**]. As an additional methodology for the study of intermolecular interactions, the Hirshfeld surfaces and fingerprint graphics are generated and illustrated in **Fig. 5**, showing surfaces that have been mapped with d_{norm}, shape index and curvedness. The d_{norm} values were mapped on the Hirshfeld surface using red, blue and white color scheme, where the red region represent the region of close contacts and blue longer contacts.

For the compound, H…Cl/Cl…H contacts that are attributed to N-H…Cl and C-H…Cl hydrogen-bonding interactions have the most significant percentage contributions to the surface of Hirshfeld 46.6% and represented by two symmetrical wings with two long and narrow points at a maximum sum of $d_e + d_i$ ~2.2 Å less than the sum of van der Waals radii of involved atoms (1.8 + 1.09 ~ 2.84), it affirms that the inter-contact are considered close.

The H…H contacts comprise 38.8% of the entire surface of Hirshfeld appear in the middle of the scattered points in the two dimensional fingerprint maps by two weak peaks around $d_e + d_i$ ~2.4 Å, a value greater than the sum of the van der Waals radii of the atoms of hydrogen (1.09 + 1.09 ~ 2.18 Å). This reveals the absence of close H…H contacts.

The contacts C…H/H…C cover 10.1% of the overall surface of Hirshfeld show on its 2D graph the presence of a symmetric pair of wings around a sum ($d_e + d_i$ ~ 2.6 Å) less than

ACCEPTED MANUSCRIPT - CLEAN COPY

the sum of the van der Waals radii of the carbon (1,75 Å) and hydrogen (1.09 Å) atoms. These contacts are considered as being close contacts.

The fingerprint plots corresponding to the contacts C…C, which represent only 2.3% of the Hirshfeld surface with ($d_e + d_i$ ~3.6 Å) smaller than the sum of the van der Waals radii of the carbon atoms (3.8 Å) confirm the presence of π-π interactions in the crystalline stack. This is also confirmed by the presence of the red and blue triangles on the Shape index cartography (**Fig. 6c**) and in the plane regions delimited by a blue outline on the Hirshfeld surfaces mapped with Curvedness (**Fig. 6d**) [**27**]. Concerning the rest of the other contacts such as O…H/H…O (2%) and Cl…Cl (0.2%) has a very weak contribution on the Hirshfeld surface.

The intermolecular interactions were further evaluated by computing the enrichment ratios (ER) in order to highlight which contacts are over-represented and are likely to represent energetically strong interactions and the driving force in crystal formation [**27**]. This ratio is defined as being the ratio between the percentage of existent contacts in the crystal and the theoretical percentage of random contacts which are summed up in **Table 4**. The list of enrichment ratios shows the contacts H...Cl/Cl...H (ER_{HCl} = 1.45) clearly supply evidence of the formation of hydrogen bonds of type N-H...Cl and O-H...Cl. The H…H contacts present the most second high percentage of contribution on the surface of Hirshfeld due to the large amount of hydrogen on the crystal packing (68.15 %), but they have too small degree appeared with an enrichment ratio 0.83. The O…H/H…O contacts represent less than 2.5% of the contact surface but are, by far, the second largest enriched at ER_{OH}=1.44, due to extensive parallel displaced stacking between cations. The C…H/H…C largest hydrogen bonds constitute the third greatest interaction surface and have the third greatest enrichment (ER_{CH} = 1.00). The enrichment ratio values of the last contact Cl…Cl are of little significance because of their small contributions to the global Hirshfeld Surface.

3.3. Quantum theory of atoms in molecules (QTAIMs) analysis

Atoms-In-Molecule (AIM) analysis proposed by Bader [**28, 29**] performed at the B3LYP/6-311G(d,p) level of theory to investigate various type of inter-inter and intra molecular interactionsin the studied structure. The topological parameters which are: the electron density (ρ(r)), the Laplacian ($\nabla^2\rho(r)$), the eigenvalues (λ_1, λ_2, λ_3), the ($\lambda_1/\lambda_{3)}$ ratio, the kinetic energy densities (G(r)), the total energy densities (H(r)), the potential (V(r)) and the bond energy (E_{int}) calculated by Espinosa method [**30**], give a lot of information on the properties of BCPs are shown in **Fig. 7**.

ACCEPTED MANUSCRIPT - CLEAN COPY

As can be seen from **Table 5**, the different topological properties of OXDACl compound are given. The energy density $H(r)$ and its Laplacian $\nabla^2\rho(r)$ allow deducing the nature of the interactions. While, $\nabla^2\rho(r)$ is positive, the energy density H(r) is observed is in the range of -0.00059 a.u and 0.00173 a.u at the CP of binding, they are mainly electrostatic and the distance between the interacting atoms is greater than the sum of the van der Waals rays of these atoms, so is indicative of the existence of weak and medium hydrogen bonds. Our study shows that the bond critical points are located in all bonds. BCP analysis shows that 15 bonds are considered as weak and 3 are considered as medium hydrogen bonds, based on Rozas et al. [**31**]. The AIM analysis reveals that our material is stabilized by 18 hydrogen bonds that meets Koch and Popelier criteria [**32**] and that $Cl_{25}…H_2$, $Cl_{26}…H_{23}$, $Cl_{26}…H_{20}$, $Cl_{27}…H_{16}$, $Cl_{31}…H_{22,}$ $Cl_{31}…H_7$ and $O_{28}…H_7$ interactions present symmetrical topological properties to $Cl_{25}…H38$, $Cl_{26}…H_{54}$, $Cl_{26}…H_{51}$, $Cl_{27}…H_{24}$, $Cl_{31}…H_{53,}$ $Cl_{31}…H_{38}$ and $O_{28}…H_{38}$ interactions.

To conclude we can say that the AIM analysis is used to confirm the H ... H contacts that are already observed by Hirshfeld surface analysis and to detect the presence of cycles in a molecular system.

3.4. Reduced density gradient (RDG) analysis

The Reduced Density Gradient (RDG) analysis provide graphical visualization of the regions where intra and inter non-covalent interactions (NCI). The RDG theory is based on the charge density introduced by Johnson et al. [**33]** and Contreras-Garcia et al. [**34**].

In **Fig. 8a**, the color coding scheme for 3D spatial visualization of RDG surface indicates of OXDACl: blue for attractive, red for repulsive and green for intermediate interactions. The results were carried out and plotted by using Multiwfn and VMD programs [**18, 20**]. **Fig. 8a** shows the evolution between RDG (a.u) versus sign $(\lambda_2)\rho$, where sign $(\lambda_2)\rho$ is the second eigen value of the electron density Hessian matrix. So with the sign $(\lambda_2)\rho$, we can discriminate between the three regions, when we have tried to understand the nature of strength of the different interactions presenting in our compound. The nature of interactions depends on the value of sign $(\lambda_2)\rho$, sign $(\lambda_2)\rho > 0$ for repulsive interaction, sign $(\lambda_2)\rho < 0$ for attractive interaction and sign $(\lambda_2)\rho$ nearly zero for van der Waals interaction (weak interaction).

The interactions appear in the form of green plates are attributed to van der Waals interactions, its plates are located exactly between the hydrogen and the chlorine atoms, which signify the strong attractive interaction N-H…Cl and C-H…Cl (**Fig. 8b**). The elliptic red plate

ACCEPTED MANUSCRIPT - CLEAN COPY

situated at the center of two rings which separated by a distance equal to 3.843 Å, is related to π-π stacking interactions between the pyridine rings and describe a strong steric effect. Then, the electron density values of 0.006–0.022 a.u correspond to steric repulsion effect between chlorine and hydrogen atoms in OXDACl.

These results confirm the presence of strong hydrogen bond interaction between solvent and molecule and are consistent with that of the AIM analysis.

3.5. Molecular electrostatic potential (MEP)

The Molecular Electrostatic Potential (MEP) surface gives information about the interaction energy between the electric charge produced by the electrons and the nuclei around the molecule. Moreover, MEP surface help us to identify the reactivity of wide variety of chemical systems in both electrophilic and nucleophilic reactions and hydrogen bonding interactions [**35**]. To predict reactive sites for electrophilic and nucleophilic attack for the investigated molecule, MEP surface is plotted over optimized at B3LYP/6-31G(d,p) basis set as can be seen in **Fig. 9**. As for the molecular electrostatic potentials (MEPs), it is seen that most of the negative potentials appear to be distributed on over Cl atoms (red color) represents the most electronegative potential (electrophilic sites), while the positive potentials appear to be at H atoms (blue color) represents the most positive electrostatic potential (nucleophilic sites), whereas the green or yellow colors indicates the neutral region. This graph mapped that the nucleophilic sites are located around the hydrogen atoms and the electrophilic sites are located around the chlorine atoms. These regions give information about intermolecular interactions.

3.6. Frontier molecular orbital analysis

The highest occupied molecular orbitals (HOMOs) and the lowest-lying unoccupied molecular orbitals (LUMOs) are named as frontier molecular orbitals (FMOs) which play an excellent role to indicate the transfer of electron in molecular systems. The energy gap ΔE between HOMO and LUMO determines the kinetic stability, chemical reactivity and, optical polarizability and chemical hardness–softness, and also good indicators of the chemical stability of a molecule. In fact, the frontiers orbitals of the HOMO’s levels indicate a charge distribution on the Cl atoms. On the other hand, the LUMO's levels present a charge distribution on the organic group.

ACCEPTED MANUSCRIPT - CLEAN COPY

The HOMO and LUMO graphics that can be observed by using Gauss View program [**16**] are mapped in **Fig. 10** in which red and green regions represent positive and negative phase, respectively.

The energies, electron affinity, global electrophilicity index, ionization potential (IP), global hardness and global softness of the most important orbital such as the HOMO (HOMO-1) and LUMO (LUMO+1) orbitals are calculated by TD-B3LYP method using the 6-311 ++ G (d,p) basis and are listed in **Table 6**.

Using the HOMO and LUMO orbital energies, the ionization potential and the electron affinity are respectively expressed as follows: A= $-E_{LUMO}$ = 2.239 eV, I= $-E_{HOMO}$ = 5.447 eV corresponding to HOMO-LUMO gap of 3.208224 eV and HOMO-1-LUMO+1 gap of 3.54591757 eV. Some relevant examples presenting band gaps ranging from 3.1739 to 3.2803 eV are given in the literature [**36**]. The electronegativity is χ is defined by Mulliken [**37**] as follows $\chi = \frac{(I + A)}{2}$. The chemical hardness and softness are determined by the following relationships $\eta = \frac{(I-A)}{2}$ and $S = \frac{1}{2\eta}$.

Moreover, Parr et al. [**38**], proposed the global electrophilicity index of a ligand as $\omega = \frac{\mu 2}{2\eta}$, were μ is the chemical potential defined by $\mu = \frac{-(I + A)}{2}$. The electrophilicity index provides insight into almost every arena of chemistry and encompasses information about the structure, properties, stability, reactivity, interactions, bonding, toxicity, and dynamics of many electron systems in ground and excited electronic states. Thus the high value of electrophilicity index **Table 6** of our compound favors its powerful electrophilic behavior. Also it seen that the chemical potential is negative it means that our crystal is stable, which is important in understanding a diverse class of biophysicochemical processes.

To conclude, from the above values, we can see that the value of the gap energy is an index of high kinetic stability and low chemical reactivity, because it is energetically unfavorable to add electron to a high-lying LUMO or to extract electrons from a low-lying HOMO.

3.7. UV–vis absorption and fluorescence properties

The solid-state UV–Vis spectrum of crystalline OXDACl measured at room temperature is shown in Fig. 11(a). The absorption spectrum exhibits one distinct absorption band centered at 290 nm. This band is attributed to the π–π* transition of the aromatic ring in o-xylylenediaminium, which is relative to the aromatic conjugation in the cations according to the literature [**21, 39**].

ACCEPTED MANUSCRIPT - CLEAN COPY

The optical band gap energy is determined by the Tauc method [**40**] by plotting $(\alpha h\upsilon)^2$ versus hυ as shown in Fig. 11(b)**.** The evaluated band gap of our compound was found to be 3.58 eV, suggesting that the crystal may possess dielectric behavior to induce polarization when powerful radiation is incident on the material [**41**].

The photoluminescence properties was studied by Perkin Elmer LS55 spectrophotometer and determined in the solid-state at room. The obtained emission spectrum (Fig. 11(c)) exhibits a peak in increasing order of intensity at λ_{em} = 430 nm showing emission in blue region. This fluorescent maximum emission band can be attributed to the π-π* charge transitions of xylylenediammonium group [**21**].

3.8. Vibrational IR spectra and assignments

Infrared spectroscopy was used to verify the functional groups present in the crystal, and to investigate their vibrational behavior in the solid state. The IR spectrum of OXDACl measured between 400 and 4000 cm^{-1} and simulated one is using B3LYP/LanL2DZ basis set are shown in Fig. 12**,** when we observed good correlations among the experimental and predicted spectra. The distribution of the different groups was studied experimentally and the calculated one from DFT method and assigned by VEDA program [**15**] and GaussView software [**16**]. The assignments of the observed bands are based on comparisons with data previously reported for similar materials [**21**].

Brief in this work, we have tried to identify as precisely as possible the characteristic bands based on our calculations as a preliminary database and also by comparison with previous vibration studies of similar compounds found in the literature [**8**].

The bands in the high-wavenumber region, between 3445 and 3150 cm^{-1}, correspond to the stretching vibrations of the N-H and O-H groups interconnected by a system of hydrogen bonds in the crystal [**39**]. The corresponding calculated values appear at 3383 and 3058 cm^{-1}**.** The weak band at 2950 cm^{-1} corresponds to the C-H stretching mode; its theoretical peak is located at 2943 cm^{-1}. The bands at 1648 and 1588 cm^{-1} are assigned to the stretching vibrations of C=C and to the NH_3^+ asymmetric and symmetric stretching vibration modes, which are theoretically predicted at 1662 and 1578 cm^{-1} [**23**]. The bands of medium intensities observed at 1487 and 1366 cm^{-1} are ascribed to the C-H asymmetric and symmetric bending vibrations, respectively. Theoretically, these modes are predicted at 1422 and 1366 cm^{-1}. The observed bands in the 1200-1000 cm^{-1} region correspond to the valence vibrations of C-C and C-N groups; this was calculated to be found in region 1255-1080 cm^{-1}. The bands

ACCEPTED MANUSCRIPT - CLEAN COPY

in the range 1000-600 cm^{-1} can be attributed to the out of plane bending modes of C-H, N-H, and C-C groups. The corresponding bands are calculated to be found at 1006 and 599 cm^{-1}.

4. Conclusion

In conclusion, we can state that the new chloride salt has been successfully synthesized and grown at room temperature by the slow solvent evaporation method. They are investigated by experimental and theoretical physicochemical methods. The structural determination discovered that π–π, N–H…Cl and O–H…Cl are implicated in the crystal packing, as investigated by the Hirshfeld surface and topological analysis. Characterization of intermolecular interactions and crystal packing via Hirshfeld surface analysis revealed that the H…Cl/Cl…H intermolecular interactions are the most abundant contacts. The enrichment ratio allowed determining which types of contacts are over or under-represented in the crystal packing. AIM, RDG and Frontier molecular orbital analysis approach determines the nature and properties of molecular interactions and reveals clearly the different characteristics of N-H and O-H bonds to suggests the good stability of title compound. MEP mapping is determined to predict the nucleophilic and electrophilic reactions also the hydrogen bonding interactions of the molecule.

Structural and spectroscopic properties were presented as well via TD-DFT and DFT calculations. The comparison between both theoretical and experimental methods shows a good correlation. The solid-state photoluminescence measurement revealed that the salt shows a strong emission in blue region.

Acknowledgements. The authors would like to thank the Ministry of Higher Education and Scientific Research of Tunisia.

ACCEPTED MANUSCRIPT - CLEAN COPY

References

[**1**] P. Metrangolo, H. Neukirch, T. Pilati, G. Resnati, Acc. Chem. Res. 38 (2005) 386–395.

[**2**] T. Steiner, Angew. Chem. Int. Ed. 41 (2002) 48–76.

[**3**] G. R. Desiraju, T. Steiner, In The Weak Hydrogen Bond in Structural Chemistry and Biolog. Oxford University Press., (2002).

[**4**] Z. Mu, L. Shu, , H. Fuchs, M. Mayor, L. Chi, J. Am. Chem. Soc. 130 (2008) 10840–10841.

[**5**] N. J. Babu, A. Nangia, Cryst. Growth Des. 11 (2011) 2662–2679.

[**6**] B. C. Felix-Sonda, J. Rivera-Islas, D. Herrera-Ruiz, H. Morales-Rojas, H. Hopfl, Cryst. Growth Des. 14 (2014) 1086–1102.

[**7**] E.T. Michalson, J. Szmuszkovicz, Medicinal agents incorporating the 1,2-diamine functionality, Prog. Drug Res. 33 (1989) 135-149.

[**8**] V. Murugesan, M. Saravanabhavan, M. Sekar, Synthesis, spectral, structural characterization and biological investigation of m-Xylylenediaminium bis(ptoluenesulfonate) monohydrate, J. Photochem. Photobiol., B 148 (2015) 358-365.

[**9**] Bruker, APEX2, SAINT and SADABS, Bruker AXS Inc, Madison, Wisconsin, USA, 2006.

[**10**] G.M. Sheldrick, Crystal structure refinement with SHELXL, Acta Cryst. C 71 (2015) 3–8.

[**11**] L.J. Farrugia, WinGX and ORTEP for windows: an update, J. Appl. Cryst. 45 (2012) 849–854.

[**12**] K. Brandenburg, Diamond Version 2.0 Impact, GbR, Bonn, 1998.

[**13**] M.J. Frisch, et al., GAUSSIAN 09, Revision A.02, Gaussian, Inc., Wallingford, CT, 2009.

[**14**] A.D. Becke, Becke's three parameter hybrid method using the LYP correlation functional, J. Chem. Phys. 98 (1993) 5648-5652.

[**15**] M.H. Jamróz, Vibrational Energy Distribution Analysis, vol. 4, Computer Program VEDA, Poland, 2004.

[**16**] R.I. Dennington, T. Keith, J. Millam, GaussView, Version 5.0.8, Semichem. Inc, Shawnee Mission, KS, 2008

[**17**] S.K. Wolff, D.J. Grimwood, J.J. McKinnon, D. Jayatilaka, M.A. Spackamn, Crystal Explorer 3.1, University of Westren Australia, Perth, 2013.

ACCEPTED MANUSCRIPT - CLEAN COPY

[**18**] T. Lu, F. Chen, Multiwfn: a multifunctional wavefunction analyzer, J. Comput. Chem. 33 (2012) 580–592.

[**19**] P.S.V. Kumar, V Raghavendra, V. Subramanian, Bader's Theory of Atoms in Molecules (AIM) and its Applications to Chemical Bonding, J. Chem. Sci. 128 (2016) 1527–1536.

[**20**] W. Humphrey, A. Dalke, K. Schulten, VMD-visual molecular dynamics, J. Mol. Graph. 14 (1996) 33–38.

[**21**] S. Gatfaoui, N. Issaoui, S. A. Brandán, T. Roisnel, H. Marouani. Synthesis and characterization of p-xylylenediaminium bis(nitrate). Effects of the coordination modes of nitrate groups on their structural and vibrational properties, J.Mol.Struct., 115 (2018) 1152–168.

[**22**] H. Cheng, H. Li. (m-Phenylenedimethylene) diammonium dichloride, Acta Cryst E64 (2008) o2060.

[**23**] I. Jomaa, O. Noureddine, S. Gatfaoui, N. Issaoui, T. Roisnel, H. Marouani, Experimental, computational, and in silico analysis of $(C_8H_{14}N_2)_2[CdCl_6]$ compound, J. Mol. Struct., 1213 (2020) 128186.

[**24**] S. Gatfaoui, H. Dhaouadi, T. Roisnel, M. Rzaigui, & H. Marouani, m-Xylylenediaminium dinitrate, ActaCryst., E70 (2014) o398-o399

[**25**] J.J. McKinnon, A.S. Mitchell, M.A, Spackman, Hirshfeld surfaces: a new tool for visualising and exploring molecular crystals, Chem. A Eur. 4 (1998) 2136.

[**26**] M.A. Spackman, J.J. McKinnon, Fingerprinting intermolecular interactions in molecular crystals, CrystEngComm 4 (2002) 378.

[**27**] C. Jelsch, K. Ejsmont, L. Huder, The enrichment ratio of atomic contacts in crystals, an indicator derived from the Hirshfeld surface analysis, IUCrJ 1 (2014) 119-128.

[28] R.F.W. Bader, M.A. Austen, Properties of atoms in molecules: atoms under pressure, J. Chem. Phys. 107 (1997) 4271-4285.

[29] R.F.W. Bader, Atoms in Molecules: A. Quantum Theory, Oxford Univ. Press, 1990, p. 12.

[30] E. Espinosa, E. Molins, Lecomte, Hydrogen bond strengths revealed by topological analyses of experimentally observed electron densities, C. Chem. Phys. Lett. 285 (1998) 170-173.

[31] I. Rozas, I. Alkorta, J. Elguero, Behavior of Ylides containing N, O, and C atoms as hydrogen bond acceptors, J. Am. Chem. Soc. 122 (2000) 11154-11161

[32] P.L.A. Popelier, F.M. Aicken, S.E. O'Brien, Atoms in Molecules, an Introduction, Prentice Hall, 2000, pp. 143-198**.**

[**33**] E.R. Johnson, S. Keinan, P. Mori-Sanchez, J. Contreras-García, A.J. Cohen, W. Yang, J. Am. Chem. Soc. 132 (2010) 6498-6506.

ACCEPTED MANUSCRIPT - CLEAN COPY

[**34**] J. Contreras-Garcia, W. Yang, E.R. Johnson, Analysis of hydrogen-bond interaction potentials from the electron density: integration of noncovalent interaction regions, J. Phys. Chem. A 115 (2011) 12983-12990.

[**35**] A.E. Reed, F. Weinhold, Natural localized molecular orbitals, Chem. Phys 83 (1985) 1736–1740.

[**36**] M. Tahenti, S. Gatfaoui, N. Issaoui, T. Roisnel, H. Marouani, A tetrachlorocobaltate(II) salt with 2-amino-5-picolinium: synthesis, theoretical and experimental characterization, J. Mol. Struct. 1207 (2020) 127781.

[**37**] R.S. Mulliken, A new electro affinity scale; together with data on valence states and on valence ionization potentials and electron affinities, J. Chem. Phys. 2 (1934) 782-794.

[**38**] R.G. Parr, L. von Szentpaly, S. Liu, Electrophilicity index, J. Am. Chem. Soc. 121 (1999) 1922-1924.

[**39**] A. Guesmi, T. Roisnel, H. Marouani, Featuring non-covalent interactions in m-xylylenediaminium bis(perchlorate) monohydrate: Synthesis, characterization and Hirshfeld surface analysis, J. Mol. Struct. 1194 (2019) 66-72.

[40] J. Tauc, Optical properties and electronic structure of amorphous Ge and Si, Mater. Res. Bull. 3 (1968) 37-46.

[41] R. Thirumurugan, B. Babu, K. Anitha, J. Chandrasekaran, Investigation on growth, structure and characterization of succinate salt of 8-hydroxyquinoline: an organic NLO crystal, Spectrochim. Acta, Part A 140 (2015) 44-53.

ACCEPTED MANUSCRIPT - CLEAN COPY

Figure captions

Fig. 1. ORTEP drawing of $(C_8H_{14}N_2)_2Cl_4{\cdot}H_2O$ with displacement ellipsoids drawn at the 30% probability level. H atoms are shown as spheres of arbitrary radii **(a)** and the optimized molecular structure **(b)**.

Fig. 2. The packing of OXDACl viewed down the a-axis (a). Partial view of the inorganic part of OXDACl showing $[(Cl)_2H_2O]$ groups (b). The packing of OXDACl viewed down the c-axis without chloride and water molecules (c). Hydrogen bonds are denoted as dashed lines.

Fig. 3. View highlighting intermolecular interactions between organic cations π–π stacking.

Fig. 4. Hydrogen bonds in OXDACl compound.

Fig. 5. Hirshfeld surfaces mapped with d_{norm} (-0.480 - 1.090) (b) (dotted lines "red" represent hydrogen bonds), shape index (-1 - 1) (c) and curvedness (-4 - 0. 4) (d).

Fig. 6. Fingerprint plots of the main interactions in the crystal packing and percentage of atoms present in OXDACl.

Fig. 7. AIM molecular graph screening the different bond critical points (BCPs) of OXDACl calculated at DFT level. The BCPs are denoted as orange smaller balls.

Fig. 8. Representation of different types of interactions in OXDACl compound **(a)**. The map of Reduced Density Gradient (RDG) defines the interaction limits for OXDACl **(b)**.

Fig. 9. Map of the Molecular Electrostatic Potentials (MEP) surfaces of OXDACl.

Fig. 10. Frontier molecular orbital plots of OXDACl compound calculated with B3LYP/6-311++G(d,p).

Fig. 11. UV-Vis spectrum **(a)** and the energy gap according to the Tauc model **(b)** of OXDACl. Emission spectrum in the solid state at room temperature of OXDACl compound **(c).**

Fig. 12. Experimental and theoretical IR spectra of OXDACl compound.

ACCEPTED MANUSCRIPT - CLEAN COPY

(a)

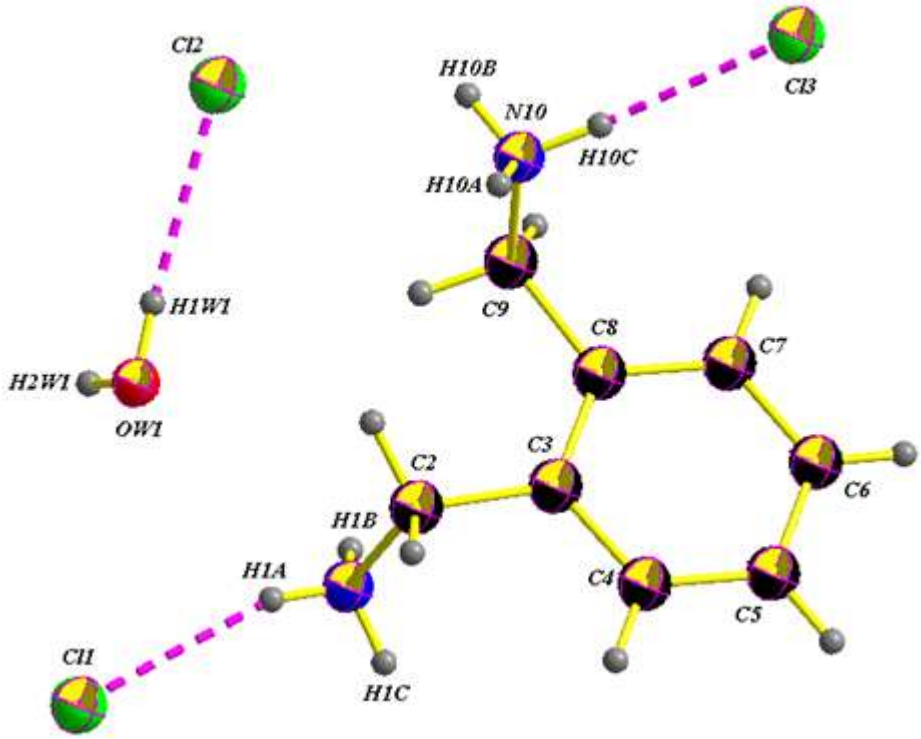

(b)

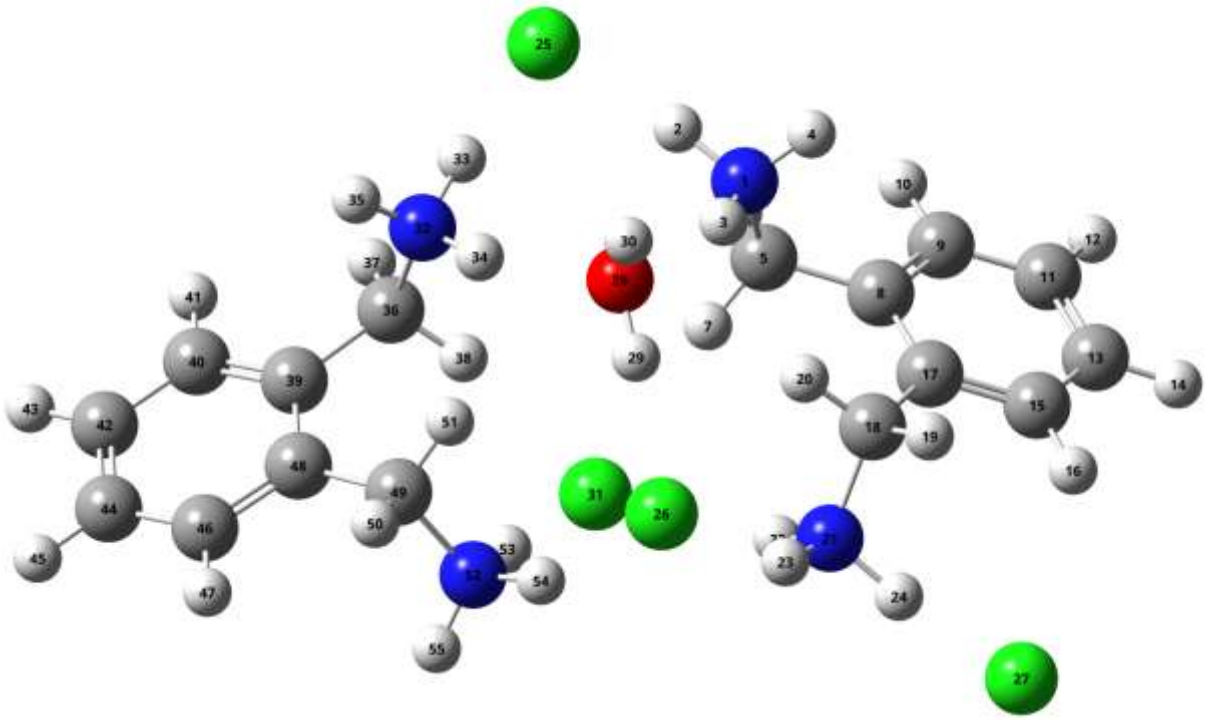

Fig. 1. ORTEP drawing of $(C_8H_{14}N_2)_2Cl_4{\cdot}H_2O$ with displacement ellipsoids drawn at the 30% probability level. H atoms are shown as spheres of arbitrary radii **(a)** and the optimized molecular structure **(b)**.

ACCEPTED MANUSCRIPT - CLEAN COPY

(a)

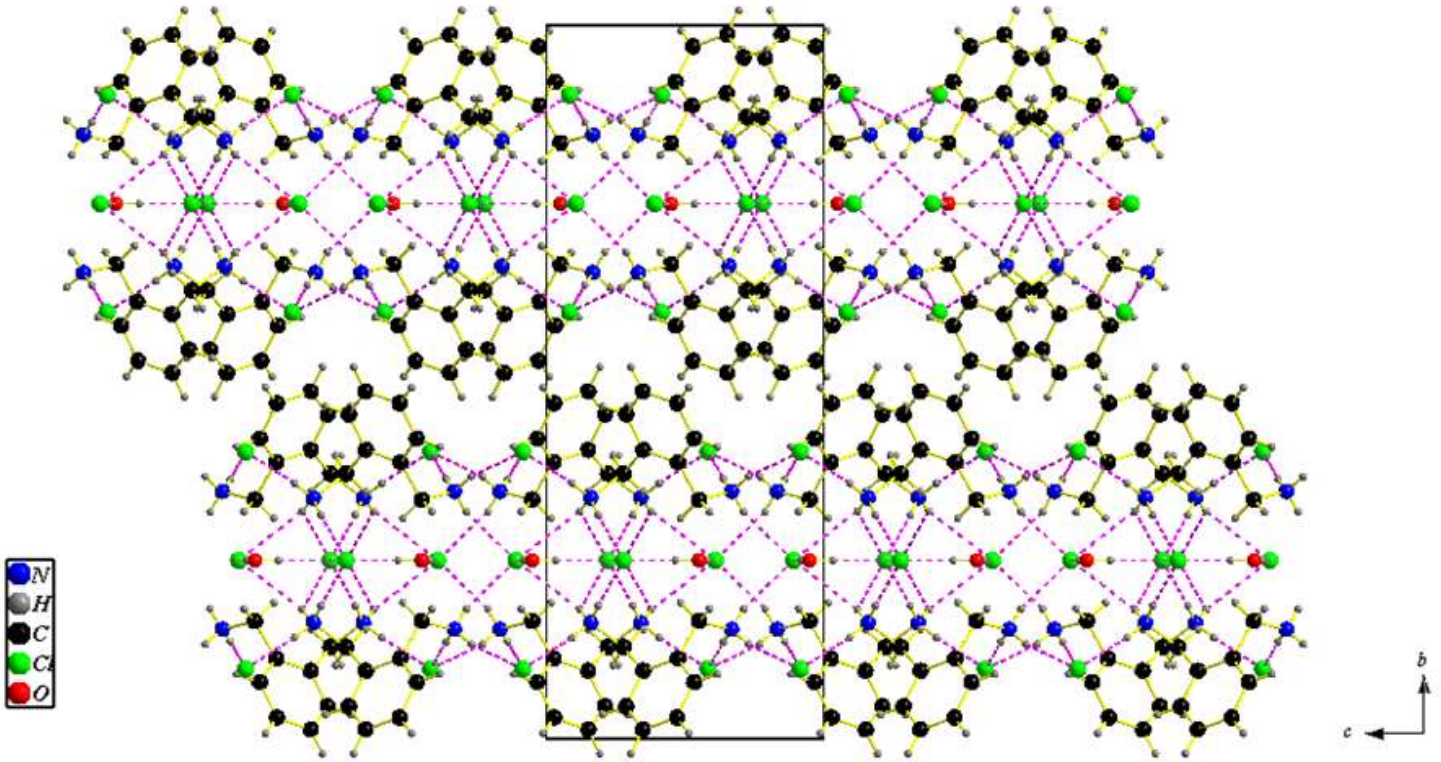

(b)

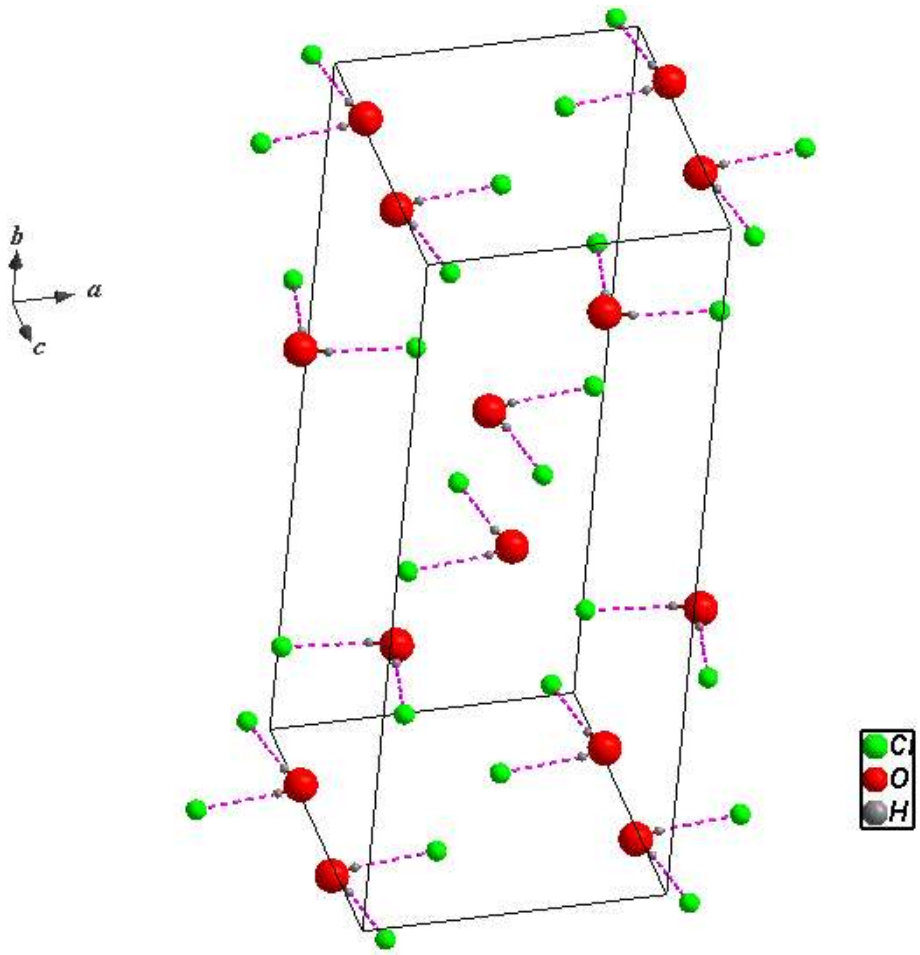

ACCEPTED MANUSCRIPT - CLEAN COPY

(c)

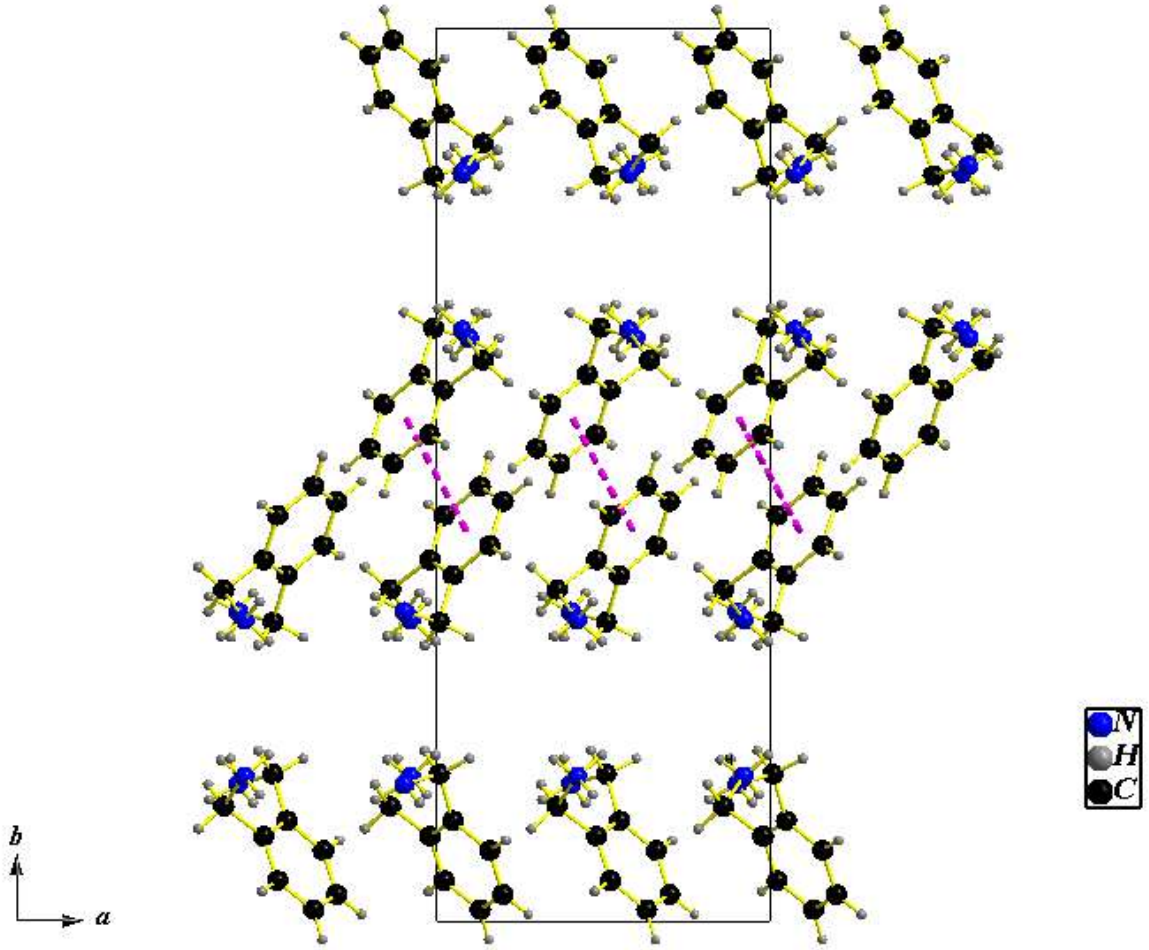

Fig. 2. The packing of OXDACl viewed down the a-axis (a). Partial view of the inorganic part of OXDACl showing [$(Cl)_2H_2O$] clusters (b). The packing of OXDACl viewed down the c-axis without chloride and water molecules (c). Hydrogen bonds are denoted as dashed lines.

ACCEPTED MANUSCRIPT - CLEAN COPY

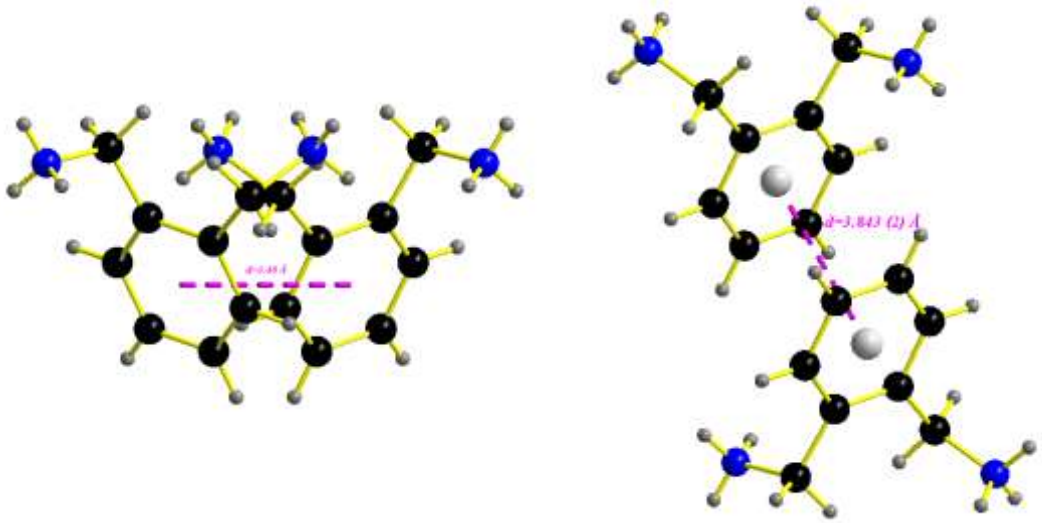

Fig. 3. View highlighting intermolecular interactions between organic cations π–π stacking.

ACCEPTED MANUSCRIPT - CLEAN COPY

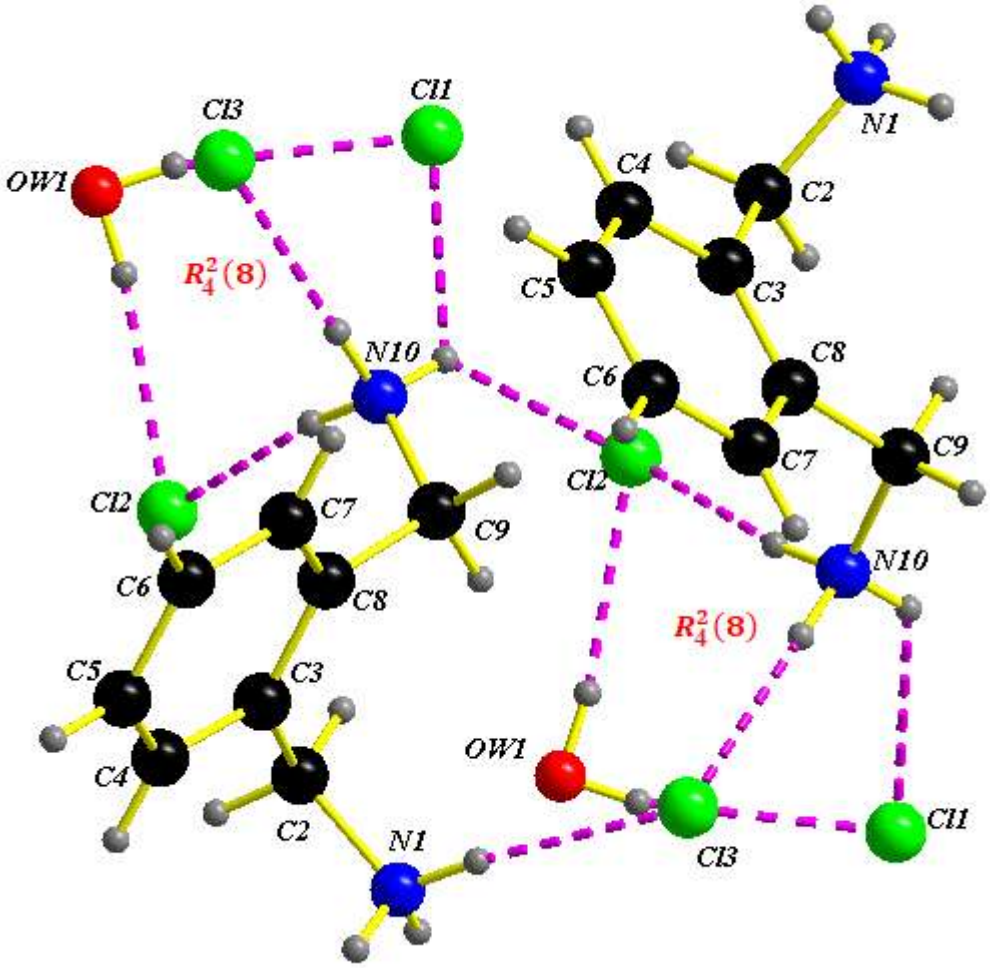

Fig. 4. Hydrogen bonds in OXDACl compound.

ACCEPTED MANUSCRIPT - CLEAN COPY

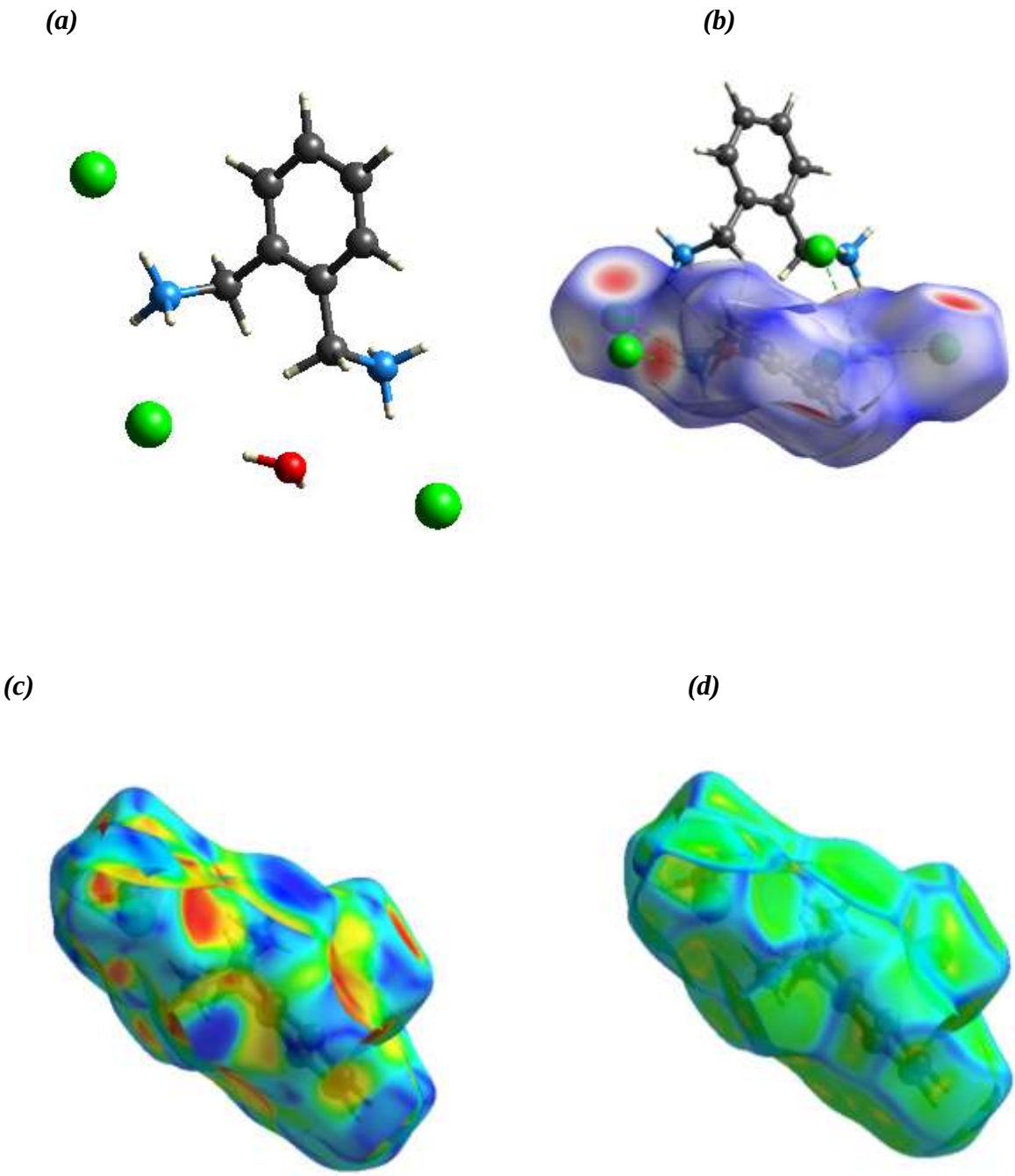

Fig. 5. Hirshfeld surfaces mapped with d_{norm} (-0.480 - 1.090) (b) (dotted lines "red" represent hydrogen bonds), shape index (-1 - 1) (c) and curvedness (-4 - 0. 4) (d).

ACCEPTED MANUSCRIPT - CLEAN COPY

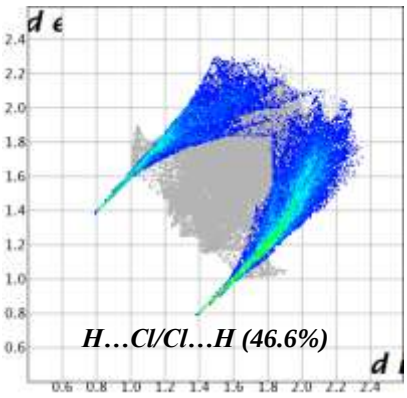

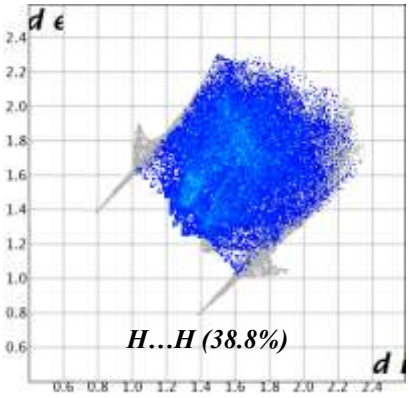

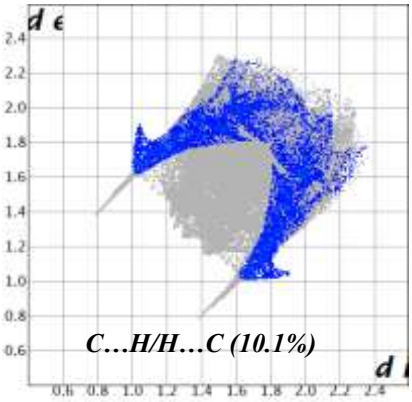

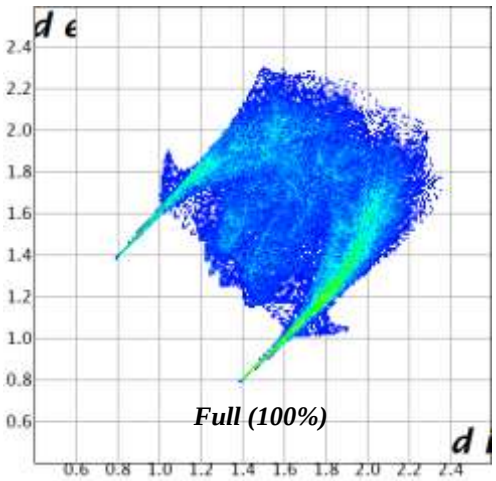

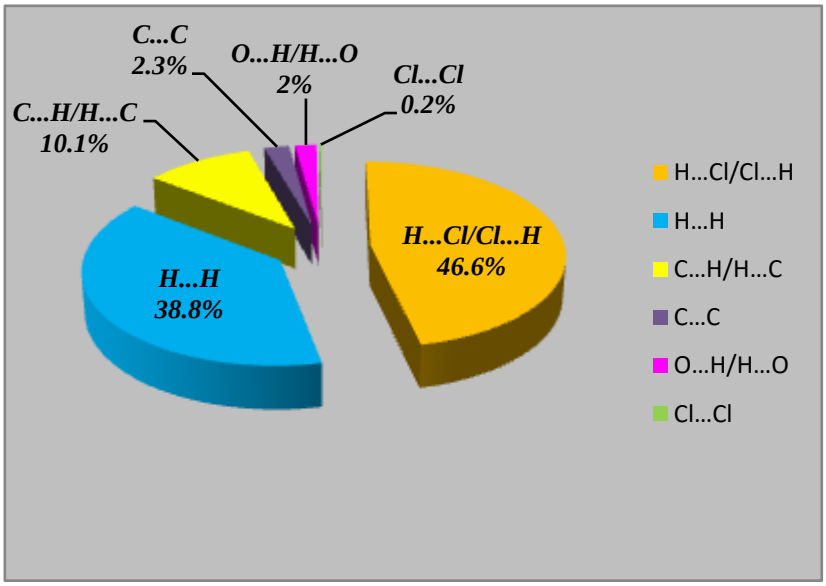

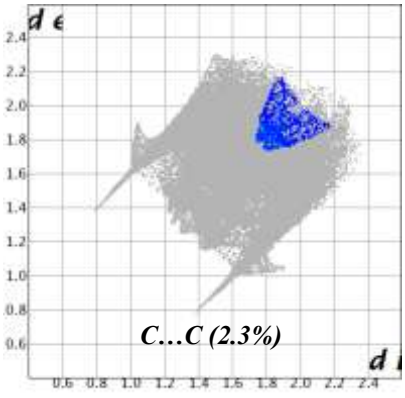

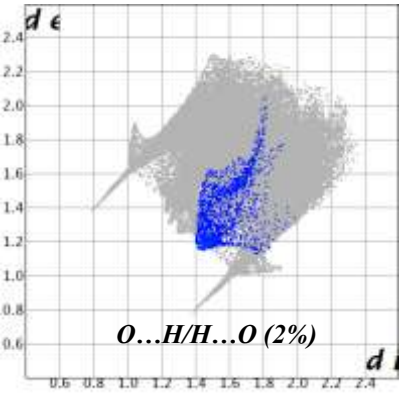

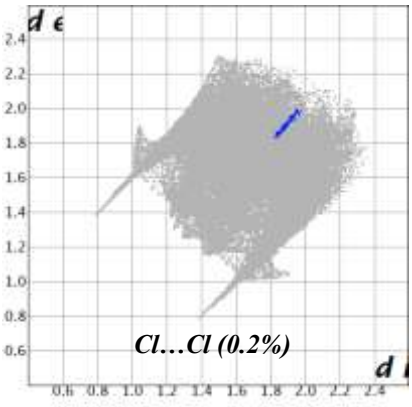

ACCEPTED MANUSCRIPT - CLEAN COPY

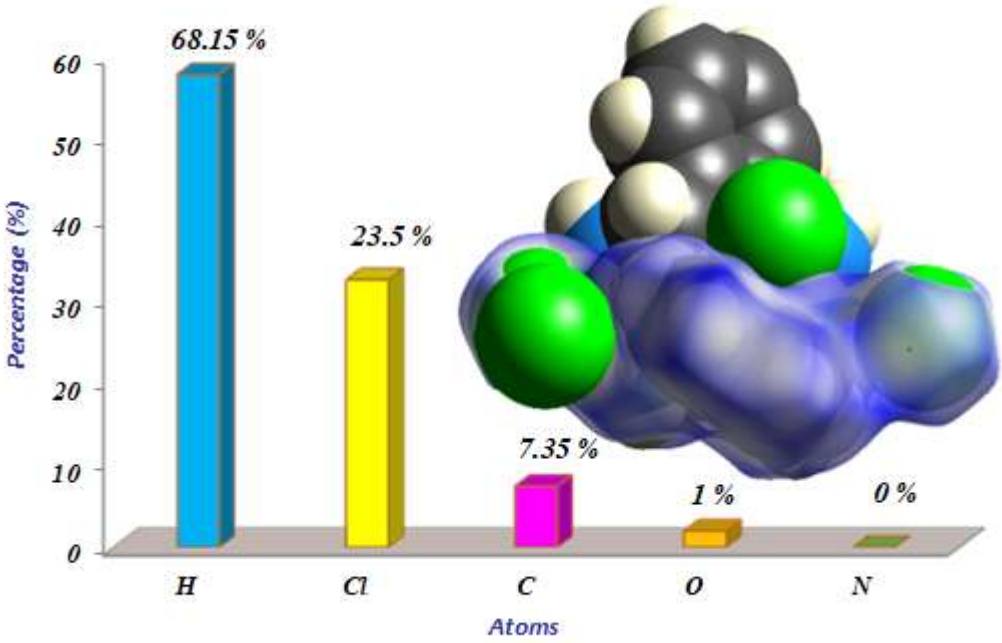

Fig. 6. Fingerprint plots of the main interactions in the crystal packing and percentage of atoms present in OXDACl.

ACCEPTED MANUSCRIPT - CLEAN COPY

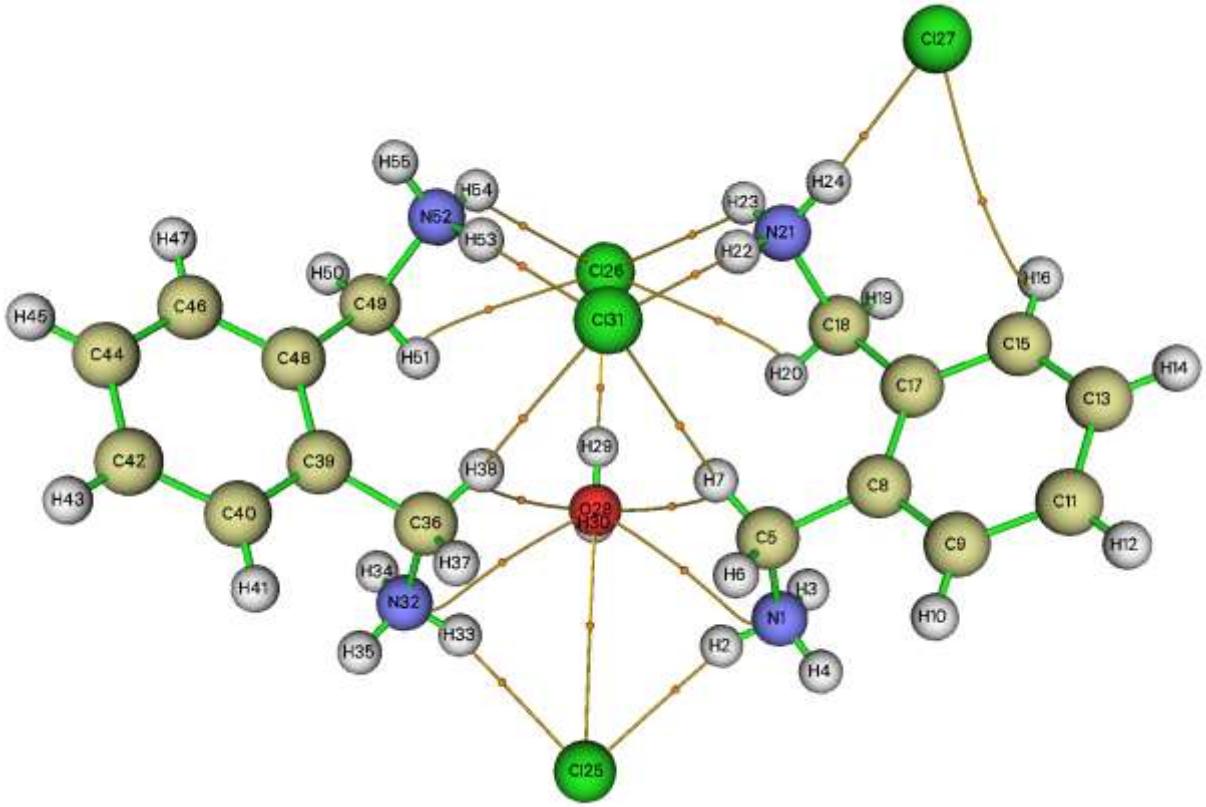

Fig. 7. AIM molecular graph screening the different bond critical points (BCPs) of OXDACl calculated at DFT level. The BCPs are denoted as orange smaller balls.

ACCEPTED MANUSCRIPT - CLEAN COPY

(a)

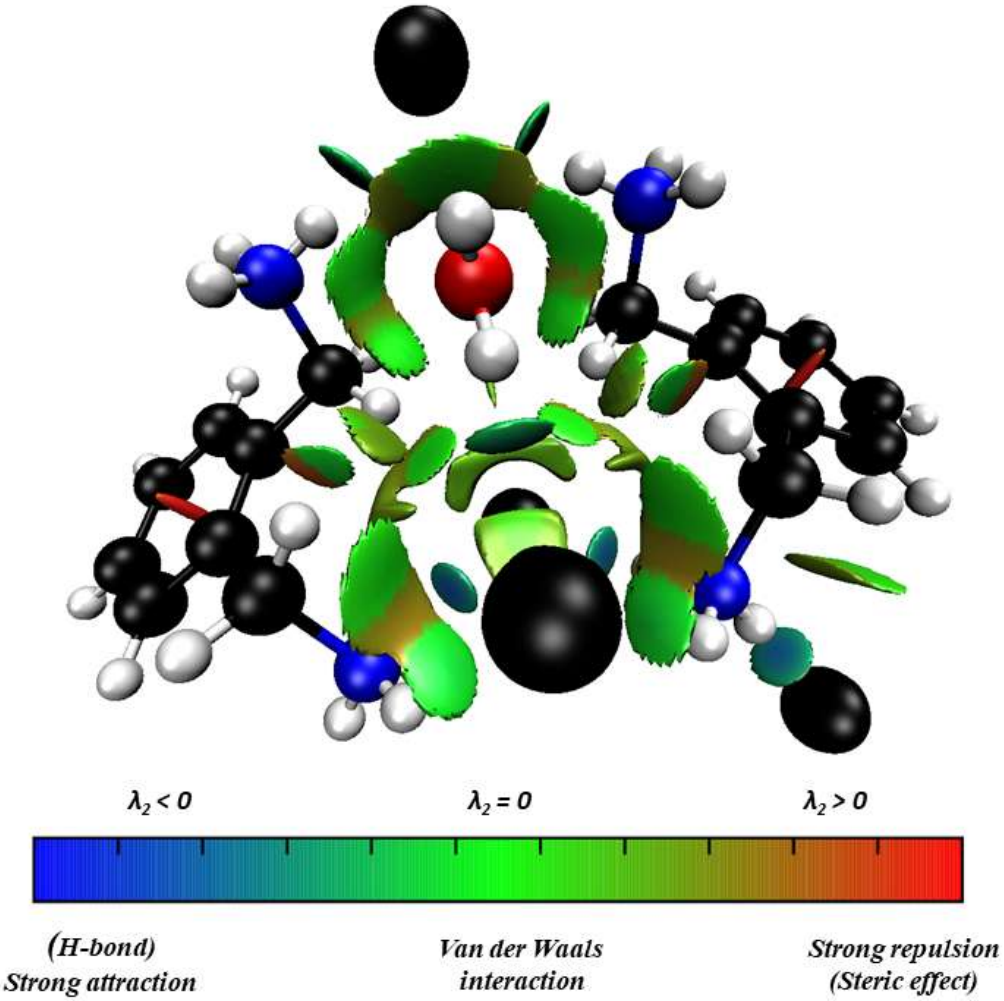

ACCEPTED MANUSCRIPT - CLEAN COPY

(b)

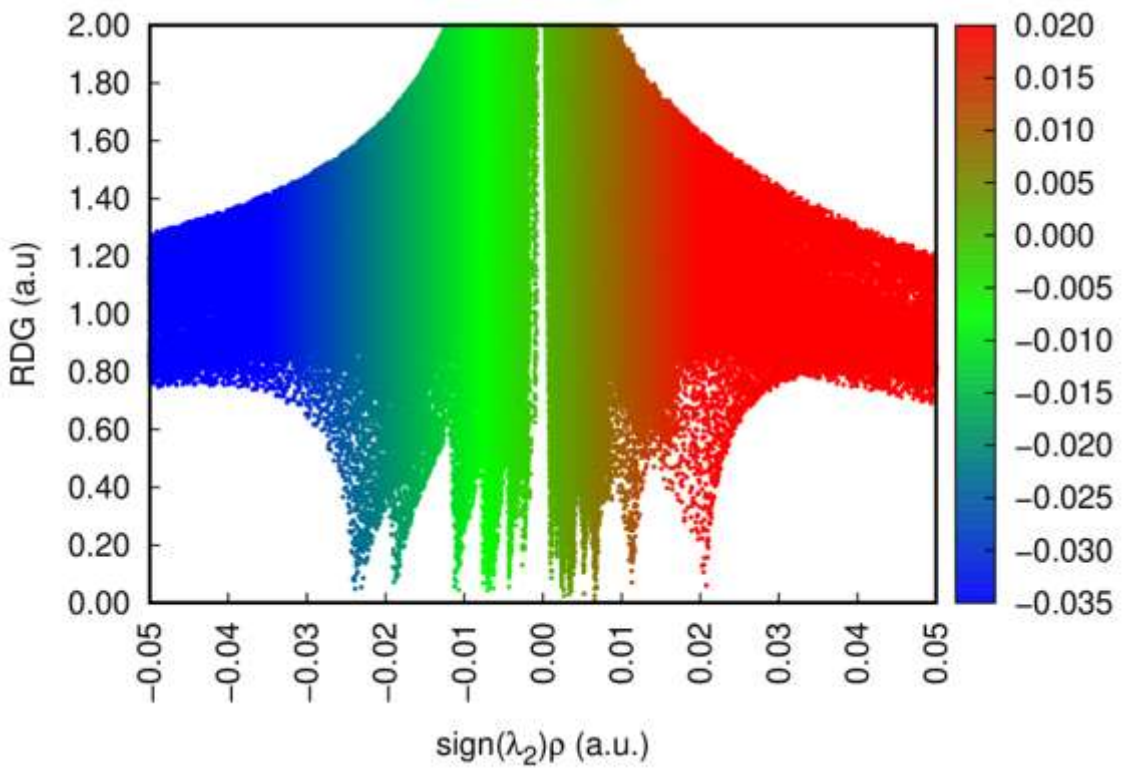

Fig. 8. Representation of different types of interactions in OXDACl compound **(a)**. The map of Reduced Density Gradient (RDG) defines the interaction limits for OXDACl **(b)**.

ACCEPTED MANUSCRIPT - CLEAN COPY

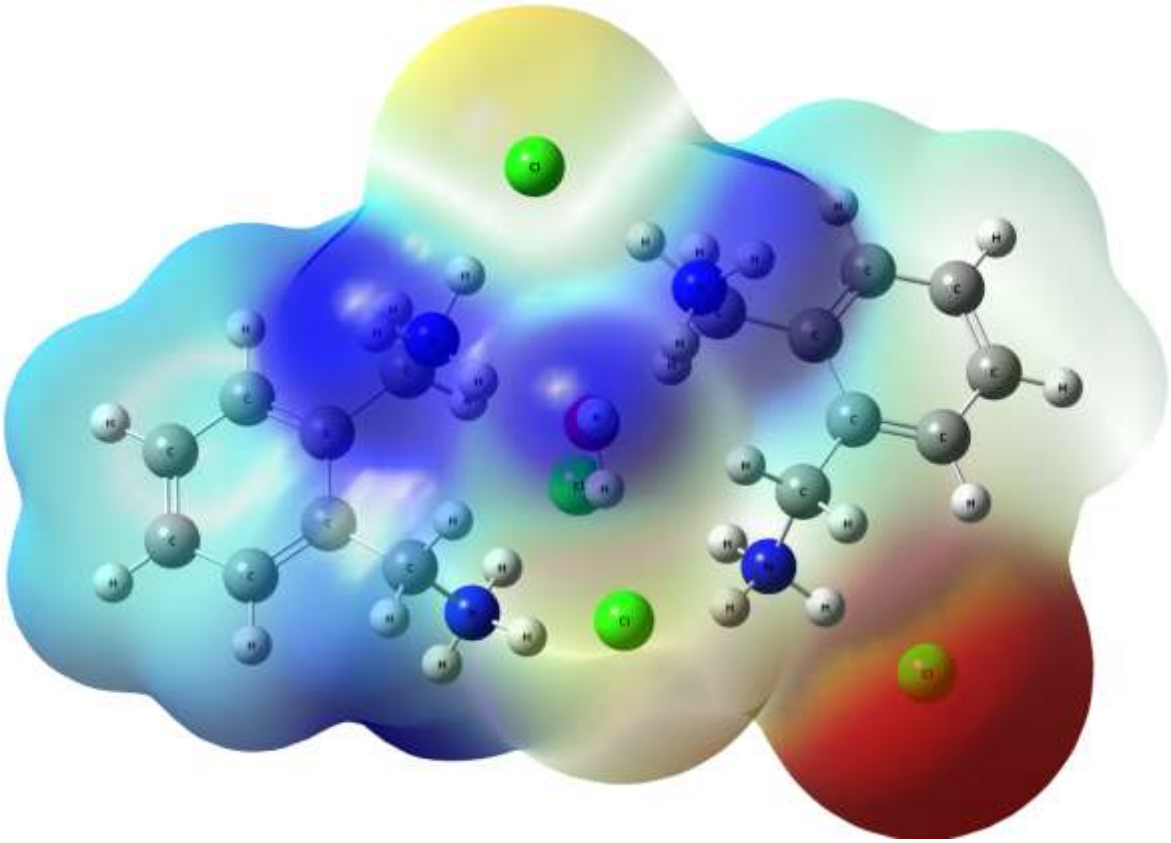

Fig. 9. Map of the Molecular Electrostatic Potentials (MEP) surfaces of OXDACl.

ACCEPTED MANUSCRIPT - CLEAN COPY

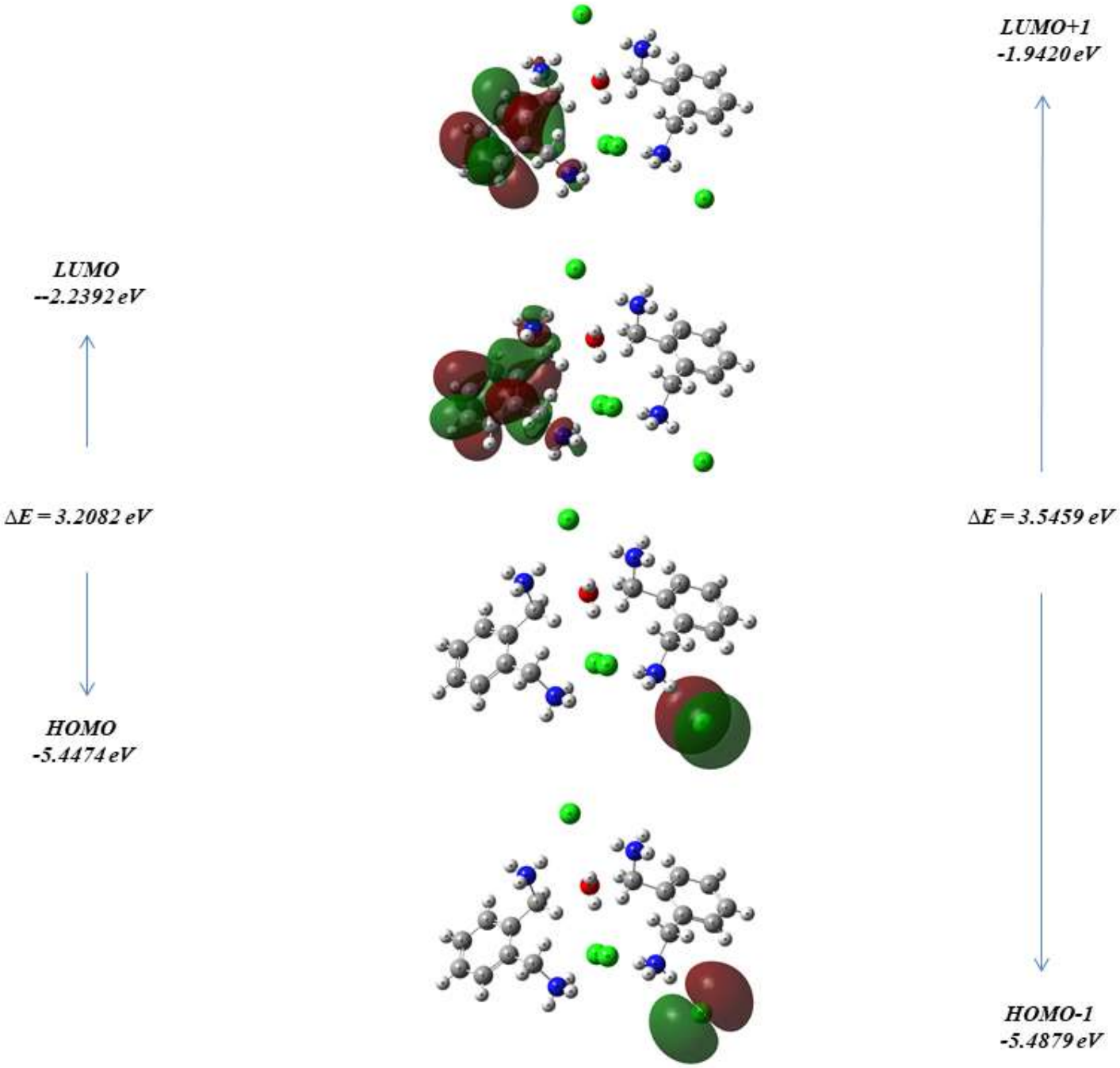

Fig. 10. Frontier molecular orbital plots of OXDACl compound calculated with B3LYP/6-311++G(d,p).

ACCEPTED MANUSCRIPT - CLEAN COPY

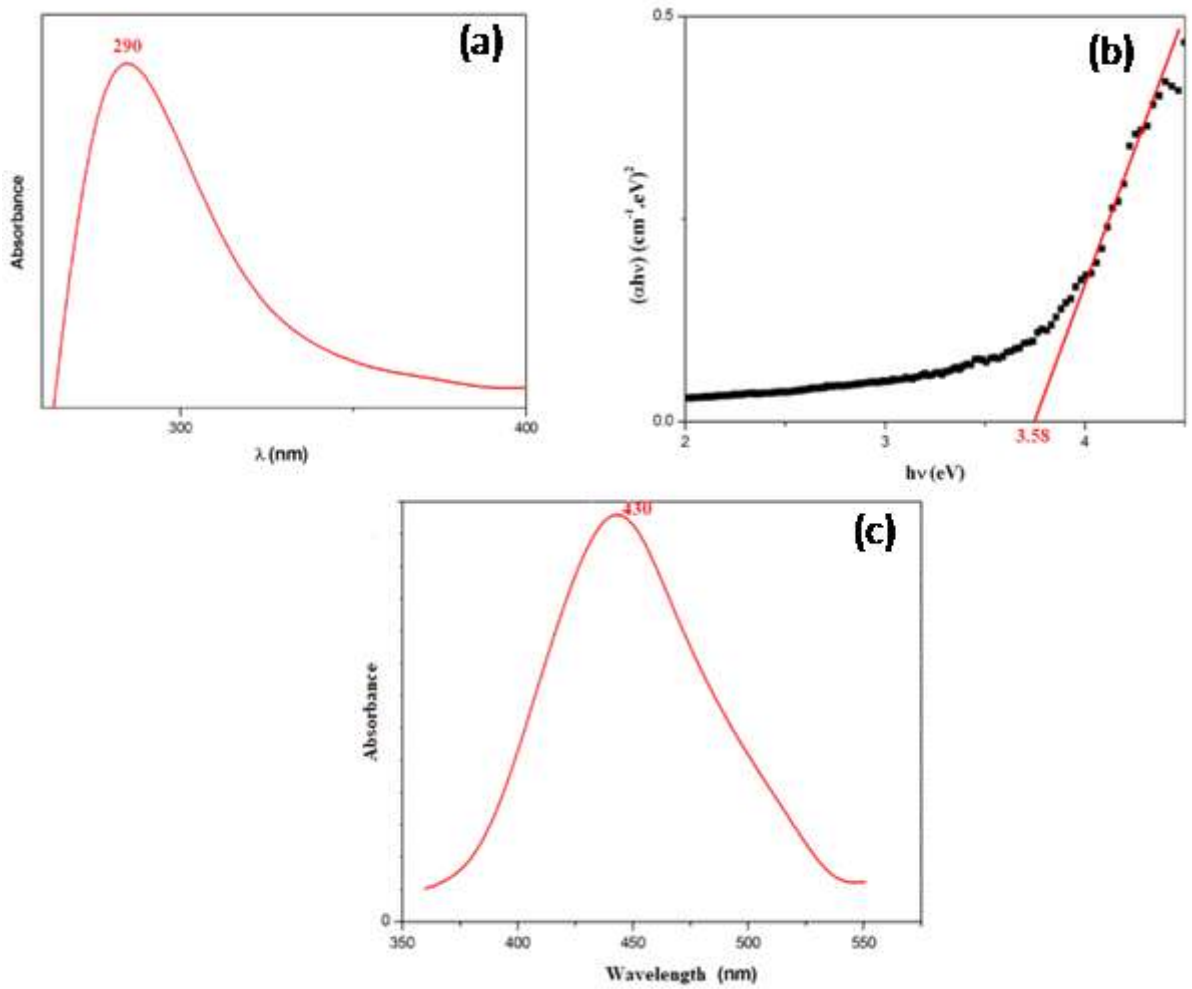

Fig. 11. UV-Vis spectrum **(a)** and the energy gap according to the Tauc model **(b)** of OXDACl. Emission spectrum in the solid state at room temperature of OXDACl compound **(c).**

ACCEPTED MANUSCRIPT - CLEAN COPY

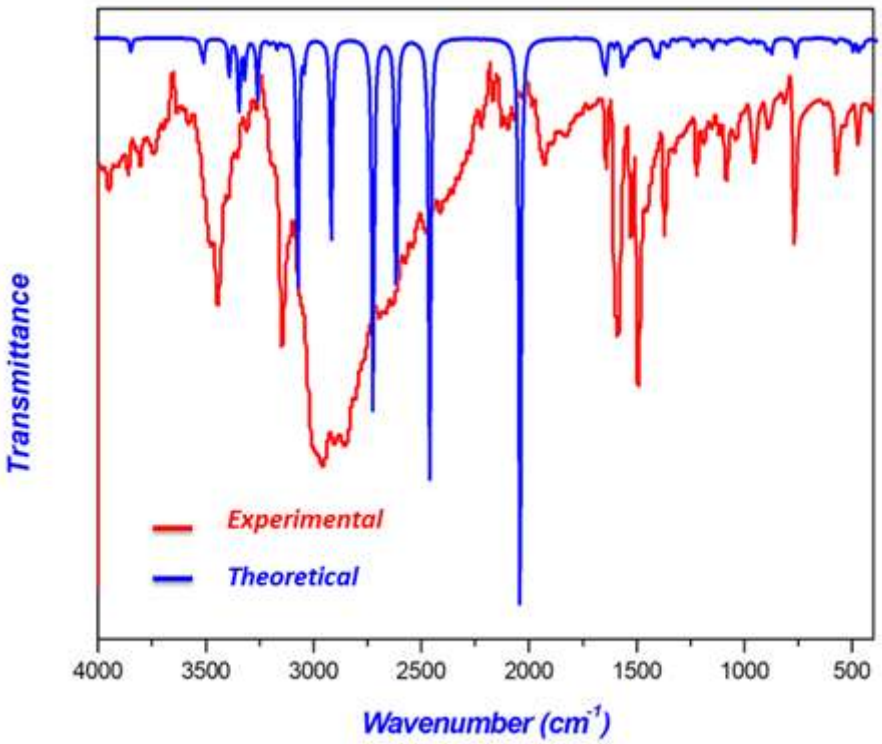

Fig. 12. Experimental and theoretical IR spectra of OXDACl compound.

ACCEPTED MANUSCRIPT - CLEAN COPY

Table captions

Table 1: Crystal data and experimental parameters used for the intensity data collection strategy and final results of the structure determination.

Table 2: Optimized and experimental bond lengths and bond angles (Å ,°) parameters of OXDACl.

Table 3: Hydrogen-bond geometry (Å, º)

Table 4: Enrichment ratio of different inter-contact and percentage of each atom on the surface Hirshfeld in $(C_8H_{14}N_2)_2Cl_4 \cdot H_2O$.

Table 5: AIM analysis of the bond critical points (BCP) for OXDACl

Table 6: Difference of energies between the possible combinations, chemical potential, Electronegativity, Global hardness, Softness and Electrophilicity. All values are in eV except for S which is given in eV^{-1}.

ACCEPTED MANUSCRIPT - CLEAN COPY

Table 1: Crystal data and experimental parameters used for the intensity data collection strategy and final results of the structure determination.

CCDC	2068832
Temperature	150K
Empirical formula	$(C_8H_{14}N_2)_2Cl_4 \cdot H_2O$
Formula weight (g mol^{-1})	436.24
Crystal system	Orthorhombic
Space group	*P*nma
a	9.0677 (9) Å
b	24.282 (2) Å
c	9.4726 (8) Å
Z	4
V	2085.7 (3) $Å^3$
F(000)	920
μ(Mo Kα)	0.71073 Å
Index ranges	$-11<h_{max}<11$, $-31<k_{max}<25$, $-12<l_{max}<12$
Reflections collected	10803
Independent reflections	2430
Reflections with I > 2σ(I)	2269
R_{int}	0.039
Absorption correction: *multi-scan*	T_{min}= 0.787, T_{max} = 0.896
Refined parameters	140
$R[F^2> 2\sigma(F^2)]$	0.032
w*R*(F^2)	0.082
Goodness of fit	1.08
$\Delta\rho_{max}$= 0.28 e $Å^{-3}$	$\Delta\rho_{min}$=-0.32 e $Å^{-3}$

ACCEPTED MANUSCRIPT - CLEAN COPY

Table 2: Optimized and experimental bond lengths and bond angles (Å ,°) parameters of OXDACl.

Bond length (Å)	***X-ray***	***Calculated B3LYP 6-311++G(d,p)***
N1-C2	1.497 (18)	1.5208
C9-N10	1.497 (18)	1.4934
C3-C4	1.396 (19)	1.4010
C3-C8	1.405 (18)	1.4106
C4-C5	1.382 (2)	1.3913
C5-C6	1.383 (2)	1.3914
C6-C7	1.387 (2)	1.3919
C7-C8	1.394 (19)	1.3999
C8-C9	1.511 (18)	1.5155
OW1-H29W1	0.851 (4)	1.0048
OW1-H30W1	0.797 (4)	0.9652

Bond angles (°)	***X-ray***	***Calculated B3LYP 6-311++G(d,p)***
H3—N1—H4	109.6 (16)	109.36
C4—C3—C2	118.3 (12)	117.34
C8—C3—C2	123.1 (12)	123.47
C4—C3—C8	118.6 (12)	119.13
C5—C4—C3	121.8 (13)	121.25
C4—C5—C6	119.3 (13)	119.48
C5—C6—C7	120.0 (13)	120.03
C6—C7—C8	121.0 (13)	121.04
C7—C8—C3	119.3 (12)	119.06
C3—C8—C9	122.5 (12)	122.80
C7—C8—C9	118.2 (12)	118.12
N10—C9—H19	109.4	109.56
N10—C9—C8	111.2 (11)	114.32
C8—C9—H20	109.4	106.97
C9—N10—H23	109.0 (12)	107.36
H22—N10—H23	108.9 (16)	106.45
H29W1-OW1-H30W1	90.3 (3)	104.03

ACCEPTED MANUSCRIPT - CLEAN COPY

Table 3: Hydrogen-bond geometry (Å, º)

D—H···A	D—H	H···A	D···A	D—H···A
N1—H1A···Cl1	0.83 (2)	2.37 (2)	3.1766 (13)	161.6 (16)
N1—H1B··· Cl3^{i}	0.926 (19)	2.317 (19)	3.2405 (14)	174.4 (14)
N1—H1C···Cl3^{ii}	0.871 (19)	2.344 (19)	3.1950 (14)	165.6 (16)
N10—H10A···Cl2^{iii}	0.923 (18)	2.264 (19)	3.1799 (13)	171.7 (15)
N10—H10C···Cl3	0.903 (19)	2.273 (19)	3.1731 (14)	174.5 (16)
OW1—H1W1···Cl2	0.85 (4)	2.35 (4)	3.197 (2)	172 (3)
OW1—H2W1···Cl1^{iv}	0.80 (4)	2.54 (4)	3.325 (2)	168 (3)

Symmetry codes: (i) x−1/2, y, −z+3/2; (ii) x, y, z−1; (iii) x+1/2, y, −z+3/2; (iv) x−1/2, y, −z+1/2.

ACCEPTED MANUSCRIPT - CLEAN COPY

Table 4: Enrichment ratio of different inter-contact and percentage of each atom on the surface Hirshfeld in $(C_8H_{14}N_2)_2Cl_4 \cdot H_2O$.

RE	H	C	O	Cl
H	0.83	1.00	1.44	1.45
C		4.26	-	-
O		-	-	-
Cl		-	-	-
% Surface	68.15	7.35	1	23.5

ACCEPTED MANUSCRIPT - CLEAN COPY

Bond critical points	Density of all electrons	Laplacian of electron density	Potential energy density V(r)	Energy density E(r) or H(r)	Interaction energy (E_{int}) $kJ.mol^{-1}$	Electron localization function (ELF)	Localized orbital locator (LOL)	Ellipticity	Eta index
$Cl_{25}…H_{2}$-N_{1}	0.01858	0.06162	-0.01376	0.00082	-17.88	0.06169	0.20419	0.00436	0.19371
$Cl_{25}…H_{38}$-N_{32}	0.01875	0.06096	-0.01375	0.00075	-17.87	0.06417	0.20763	0.00439	0.19558
$Cl_{25}…O_{28}$	0.00633	0.01909	-0.00364	0.00057	-4.73	0.02133	0.12892	0.60904	0.15173
$Cl_{26}…H_{54}$-N_{52}	0.01104	0.03982	-0.00674	0.00161	-8.76	0.03412	0.15837	0.11195	0.16416
$Cl_{26}…H_{23}$-N_{21}	0.01074	0.04079	-0.00673	0.00173	-8.75	0.03038	0.15053	0.12602	0.15938
$Cl_{26}…H_{51}$-C_{49}	0.00694	0.02291	-0.00319	0.00127	-4.15	0.02563	0.13981	0.95681	0.14823
$Cl_{26}…H_{20}$-C_{18}	0.00671	0.02305	-0.00318	0.00129	-4.13	0.02283	0.13284	1.03444	0.14590
$Cl_{27}…H_{24}$-N_{21}	0.02389	0.06605	-0.01764	-0.00056	-22.93	0.09980	0.24991	0.00410	0.22183
$Cl_{27}…H_{16}$-C_{15}	0.00434	0.01202	-0.00162	0.00069	-2.11	0.01988	0.12514	0.58602	0.12972
$Cl_{31}…H_{22}$-N_{21}	0.02307	0.07057	-0.01785	-0.00011	-23.21	0.08368	0.23217	0.00423	0.21312
$Cl_{31}…H_{53}$-N_{52}	0.02419	0.06669	-0.01785	-0.00059	-23.21	0.10162	0.25178	0.00431	0.22413
$Cl_{31}…H_{7}$-C_{5}	0.00687	0.02376	-0.00313	0.00141	-4.06	0.02397	0.13575	0.12110	0.14216
$Cl_{31}…H_{38}$-C_{36}	0.00709	0.02387	-0.00319	0.00139	-4.15	0.02613	0.14101	0.13050	0.14305
$Cl_{31}…H_{29}$-O_{28}	0.01906	0.06034	-0.01426	0.00041	-18.54	0.06602	0.21014	0.02135	0.20290
$O_{28}…N_{1}$	0.00759	0.03281	-0.00548	0.00136	-7.13	0.01484	0.10947	0.63954	0.13860
$O_{28}…N_{32}$	0.00764	0.03285	-0.00548	0.00136	-7.13	0.01515	0.11050	0.64861	0.13920
$O_{28}…H_{7}$-C_{6}	0.00704	0.02833	-0.00463	0.00123	-6.02	0.01573	0.11241	0.51088	0.15585
$O_{28}…H_{38}$-C_{36}	0.00702	0.02839	-0.00461	0.00125	-5.99	0.01562	0.11203	0.54506	0.15583

Table 5: AIM analysis of the bond critical points (BCP) for OXDACl

ACCEPTED MANUSCRIPT - CLEAN COPY

Table 6: Difference of energies between the possible combinations, chemical potential, Electronegativity, Global hardness, Softness and Electrophilicity. All values are in eV except for S which is given in eV^{-1}.

Parameters	
E_{HOMO}	-5.44745
E_{LUMO}	-2.239226
Energy Band Gap (ΔE)	**3.208224**
E_{HOMO-1}	-5.487995
E_{LUMO+1}	-1.9420775
$\Delta E = E_{LUMO+1} - E_{HOMO-1}$	**3.54591757**
Chemical potential (μ)	-3.843338
Softness (ς)	0.802056
Ionization energy (I)	5.44745
Electron affinity (A)	2.239226
Electronegativity (χ)	3.843338
Chemical hardness (η)	1.604112
Electrophilicity index (ω)	4.604181

ACCEPTED MANUSCRIPT - CLEAN COPY